

The 6.2 μm band position in laboratory and astrophysical spectra: a tracer of the aliphatic to aromatic evolution of interstellar carbonaceous dust

T. Pino¹, E. Dartois², A.-T. Cao¹, Y. Carpentier¹, Th. Chamaillé¹, R. Vasquez¹, A. P. Jones², L. d'Hendecourt², and Ph. Bréchnac¹

¹ Laboratoire de Photophysique Moléculaire*, CNRS, UPR-3361, bâtiment 210, Université Paris-Sud, 91405 Orsay Cedex, France
e-mail: thomas.pino@u-psud.fr

² Institut d'Astrophysique Spatiale, CNRS, UMR-8617, Université Paris-Sud, bâtiment 121, 91405 Orsay Cedex, France

Received 8 April 2008 / Accepted 24 July 2008

ABSTRACT

Context. The infrared emission features observed in the mid-infrared wavelength range in astronomical objects, often called the Aromatic Infrared Bands, exhibit differences in shape and position. Three astrophysical spectral classes have been proposed based on the spectral characteristics. The band positions in most sources are similar to those of aromatic materials, however, the exact nature of the emitters is still unknown.

Aims. The spectral diversity of the bands provides a clue to the nature of the materials. An evolutionary scenario for the nature of the emitters can be inferred by comparison with laboratory analogues.

Methods. The laboratory spectra of a wide range of soot material samples were recorded and a global analysis of the infrared absorption spectra performed. This spectral analysis, allied to the band shape and position variations, were then used to interpret the diversity and evolution of the features in the astronomical spectra.

Results. We find correlations between the spectral regions characteristic of the CC and CH modes and use these to shed light on the origin of the infrared emission features. In particular, the observed shift in the position of the 6.2–6.3 μm band is shown to be a key tracer of the evolution of the aliphatic to aromatic component of carbonaceous dust.

Key words. astrochemistry – ISM: dust, extinction – ISM: general – infrared: ISM – stars: AGB and post-AGB

1. Introduction

The ubiquitous Aromatic Infrared Bands (AIBs), found principally at 3.3, 6.2, 7.7, 8.6, 11.3 and 12.7 μm are clearly tracers of a carbonaceous dust component in the interstellar medium (ISM) where the dust is subjected to UV and/or visible photon excitation. Their existence has been known since the early seventies (Gillett et al. 1973). The carriers of these emission bands are responsible for the transfer of a large fraction of the UV/visible starlight into the mid-infrared wavelength range, on average 10–15% but the fraction can be as high as 40% (Désert et al. 1990). This occurs via electronic to vibrational internal energy conversion followed by intramolecular vibrational energy redistribution and subsequent infrared fluorescence (e.g. Léger & Puget 1984; Allamandola et al. 1989; Boulanger et al. 2000). The spectral positions of the bands at 3.3, 6.2 and 11.3 μm lie very close to the C–H and C=C stretching and out-of-plane bending vibrational modes, respectively, in many polyaromatics. This pointed toward an aromatic hydrocarbonaceous character for the main component of the carriers (Duley & Williams 1981) but since then the exact nature of the carrier(s) has been difficult to determine. This is partly due to the inherent complexity of hydrocarbon materials as well as the many physical processes that govern the IR emission process.

* Laboratoire associé à l'Université Paris XI, et à la Fédération de recherche Lumière Matière.

Spectroscopic observations performed by ISO (Peeters et al. 2002; van Diedenhoven et al. 2004), Spitzer (Sloan et al. 2005; Flagey et al. 2006; Draine & Li 2007) and ground-based observatories (Geballe et al. 1992; Joblin et al. 1996; Goto et al. 2002, 2003, 2007; Hrivnak et al. 2007) have revealed the spectral diversity of the observed AIBs. This has resulted in their general classification into three major groups: A, B and C (Peeters et al. 2002; van Diedenhoven et al. 2004). The most striking variations at the heart of these classes are: (i) a progressive shift of the so-called “6.2 μm ” emission band from 6.2 to 6.3 μm from class A to C, and (ii) a shift of the “7.7 μm ” double peaked feature toward 8 μm , concomitant with a progressive merging with the 8.6 μm feature into a single and much broader band. The distribution of the sources characteristic of the three classes shows that the most commonly observed class is, by far, class A. Class A sources are evenly distributed over many sorts of astrophysical objects in the galaxy, whereas class C sources are rare in comparison. Nevertheless, the observed spectral variations between and within the three classes should help to delineate the carrier characteristics that will enable us to decipher the chemical nature and evolution of interstellar carbonaceous dust.

The observed shift of the band at 6.2 μm towards 6.3 μm was recently assigned by Hudgins et al. (2005) to the presence of nitrogen heteroatoms in an otherwise pure polyaromatic structure. The change in the local bonding configuration around the N atom induces a wavelength red-shift that depends

on the N atom substitution site within the aromatic structure. Alternatively, using Spitzer spectrographic observations of the carbon star HD 100764, Sloan et al. (2007) propose that a mix of aliphatics and aromatics in the same carriers might explain this behaviour and could further explain the nature of the class C spectrum.

Spitzer observations have brought important and critical information to bear on the structural nature of the hydrocarbon carriers in the ISM of luminous IR galaxies (Dartois & Muñoz-Caro 2007; Dartois et al. 2007). These works critically showed that in these objects the hydrocarbons observed in absorption contain only a relatively minor fraction of aromatic CH bonds. In our own galaxy the interstellar hydrocarbon grains observed in the diffuse ISM also contain an important aliphatic carbon dust component that is hard to observe and characterise (Sandford et al. 1991; Pendleton & Allamandola 2002).

In a comprehensive and multidisciplinary effort to understand the observed astronomical AIB spectral classes we present the first spectroscopic results of a dedicated experiment aimed at producing, studying and characterising laboratory analogues of interstellar hydrocarbon nanoparticles. The paper is organised as follows: Sect. 2 describes the experimental set-up, the measurements and the main results concerning the physical, chemical and structural interpretation of the infrared spectra of the as-produced carbon dust analogues. The selection of astronomical spectra and data reduction that we have used for direct comparison are given in Sect. 3. The comparison of the analogues with astronomical spectra and the correlations are presented in Sect. 4. We then discuss the nature of the carriers and their consequences for carbonaceous dust evolution in the ISM. Finally, we give some perspectives for the possible further developments opened up by this work.

2. Laboratory study of soots

2.1. Experiment

The experimental set-up, at the Laboratoire de Photophysique Moléculaire in Orsay, is devoted to the production and spectroscopic analysis of laboratory analogues of carbonaceous cosmic dust. It combines a reactor chamber (working at about 50 mbar) and a sampling chamber (at a pressure of a few 10^{-2} mbar) where a molecular jet seeded with the reactor products is formed (Fig. 1). The reactor products were deposited onto a substrate placed in the molecular jet for in- and ex-situ analysis. A time-of-flight (TOF) mass spectrometer can be used for the mass analysis of the free-flying products. In the present work, the TOF was not used. Only a brief description will be given here as a detailed description of the experimental set-up will be given in a forthcoming paper.

2.1.1. Production of carbonaceous materials

The reactor chamber is equipped with a low pressure, flat and premixed flame (Fig. 1). This type of flame is considered as a model system for the physical and chemical study of combustion processes. It displays the peculiar property of offering a one-dimensional reactor where the axis normal to the plane of the burner is in fact directly linked to the chemical evolution time (Bockhorn 1994; Homann 1998; D'Anna et al. 2000; Richter & Howard 2000). Such a reactor has already been used in the context of cosmic dust analogue production but mainly for studies of the interstellar UV bump region (217 nm) in the spectra of soot samples (Schnaiter et al. 1996). The soot produced in burning

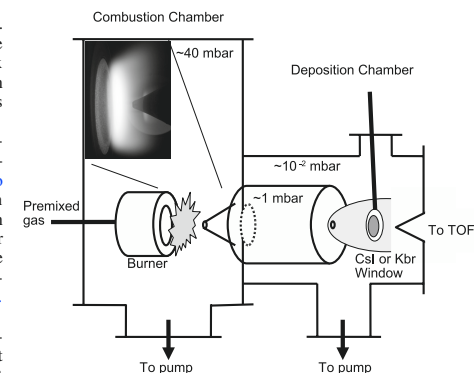


Fig. 1. A schematic view of the experimental set-up that was used. The combustion chamber contains the flat burner, cooled by circulating water. The flame is horizontal and the flow (pre-mixed) is maintained at a constant pressure within the chamber, at about a few tens of mbar. The burner is movable along the horizontal axis. The quartz sampling cone (shown) allows species produced at a given distance from the burner to enter the copper thermalisation chamber. This chamber is placed in the deposition chamber, which is maintained at a pressure of about 10^{-2} mbar under the operating conditions. A window is then placed into the jet that is formed at the end of the thermalisation chamber, where the gas passes through the nozzle.

diffusion and/or atmospheric flames was thoroughly analysed and has been used as an astronomical laboratory analogue (Mennella et al. 1995; Buchtá et al. 1995). Other than sooting flames other types of reactors have been used, such as: laser pyrolysis (Schnaiter et al. 1999; Galvez et al. 2002; Jäger et al. 2006), photolysis (Dartois et al. 2004), laser ablation (Mennella et al. 1999), reactive plasmas (Lee & Wdowiak 1993; Scott & Duley 1996; Furton et al. 1999; Goto et al. 2000), etc. In most of these experiments the low pressure premixed flame was clearly shown to produce gas phase aromatic material in the size range of a few hundreds of carbon atoms (Homann 1998; Weilmünster et al. 1999; Keller et al. 2000; Fialkov et al. 2001). With our set-up we have investigated the possibility of producing such molecular assemblies as analogues of astrophysical hydrocarbons.

The reactor comprises a stainless steel McKenna burner mounted in a vacuum chamber pumped down to a pressure of few tens of mbar (Fig. 1). The burner has a diameter of 60 mm and is surrounded by a shroud in order to produce a column of inert gas that shields the burning gas flow. Many system parameters were explored. The pressure, in the chamber, during combustion was varied from 20 to 100 mbar. The input gas velocity was varied between 3 and 6 1 min^{-1} and the distance from the burner was in the 0–60 mm range. It should be noted that the flame is a reactive medium which requires well-constrained conditions in order that the combustion be maintained. Under the present range of conditions the combustion could be stabilized for periods of hours. The flame products were mostly sampled in the sooting zone, i.e. in the region which glows orange due to the growth and evolution of the soot at temperatures of ≈ 2000 (± 500) K. Various quartz cones, cooled by thermal contact with circulating water, and with a pinhole diameter of 0.25, 0.75 and 1 mm were used to extract, in the downstream

chamber, the soot from the flame at a given distance from the burner surface.

Several precursor hydrocarbons were used, namely acetylene C_2H_2 , ethylene C_2H_4 and propylene C_3H_6 and were premixed with O_2 in the burner. They are all capable of producing soot under rich conditions, i.e. we varied the C/O ratio in the range 0.5–2, well above the stoichiometric conditions. However, the amount of soot produced was much higher when burning acetylene as compared to the other precursors.

2.1.2. Analysis: FTIR measurements on the deposited soots

Sample deposition onto CsI or KBr substrate windows was performed in the sampling chamber pumped down to a pressure of a few 10^{-2} mbar while the burning gas was flowing. The windows were placed perpendicular to the molecular jet formed behind the nozzle and terminating in the diffusion chamber (Fig. 1). The latter chamber (pressure about 1 mbar) was directly fed with the products extracted from the flame. This enables a collisional cooling of the species, by the low temperature inert gas, to roughly room temperature before expansion and deposition. Nozzles of diameters from 2 to 10 mm were used. The deposition time was adjusted in order to optimize the sample thickness (typically up to a few microns) deposited on the substrate.

After deposition, the infrared absorption spectra were measured in transmission in the 2–15 μm range, using two different configurations. In some cases a commercial Bruker Vector 22 infrared spectrometer was coupled to the sampling chamber for in-situ infrared absorption measurements. However, in most cases, the samples were measured ex-situ by Fourier Transform Infrared microspectroscopy (μ -FTIR) using a Nicolet Magna-IR 560 ESP spectrometer coupled to a Nicolet Nicplan infrared microscope. Typically 128 scans or more (at 2 or 4 cm^{-1} resolution) were acquired in order to optimize the signal-to-noise ratio. Exposure to air after deposition did not affect the samples because no contamination was observed: when measured by the two different methods, the spectra were identical. The mapping of the samples using the μ -FTIR did not reveal any clear spatial variations resulting from segregation in the jet. It showed that the samples are rather homogeneous, apart from local thickness variations that arise from the density profile in the molecular jet.

2.2. Soot spectroscopic analysis

More than 50 distinct soot samples were analysed in the present study revealing a wide variety of produced materials. Some show a continuum, increasing in intensity with decreasing wavelength. On top of this are superimposed bands typical, in shape and position, to the vibrational bands of hydrogenated carbonaceous materials. The intensity ratio between the continuum and the bands varied from sample to sample. A few samples, including those which were inferred to be dominated by aromatic units, did not show any continuum at all. The band-to-continuum ratio seems, almost always, to systematically favour the bands: the intrinsic intensities of the individual bands are found to be larger than that of the underlying continuum, except in the 3 μm region. In most cases the continuum was inferred to be due to true absorption rather than to scattering.

Three representative infrared absorption spectra, after subtraction of the continua (samples 1–3), is shown in Fig. 2. The continua were determined by a spline fitting of the baseline outside the main vibrational band regions for each spectrum. The spectra are presented for four spectral regions, normalized to

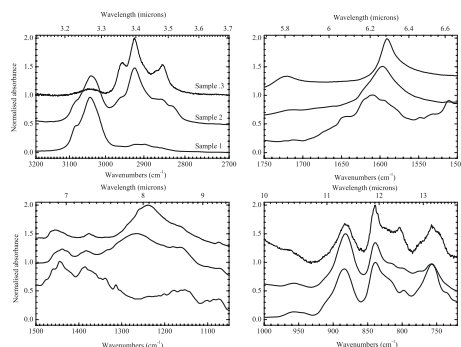


Fig. 2. Infrared absorption spectra of three different samples of laboratory soot (see the text for details). The spectra have been continuum subtracted to enhance the spectral profiles, as in Peeters et al. (2002). The spectra are presented in four spectral regions, normalized by intensity, allowing us to emphasize the band shape and position evolution within the specific frequency region. The regions are chosen to match those used previously by Peeters et al. (2002).

the intensity in each case, allowing us to emphasize the band shape and position evolution within the specific frequency regions. These regions are chosen to match those used previously by Peeters et al. (2002) in the initial AIB classification. The region around 3000 cm^{-1} corresponds to the CH stretching modes, that around 1600 cm^{-1} to the C=C stretching modes, 1500–1000 cm^{-1} to the CH bending motions and C–C stretching motions, and the 1000–720 cm^{-1} region to the CH “out-of-plane” bending motions.

A detailed analysis was performed using a deconvolution of the observed bands after subtraction of the continuum. A Gaussian lineshape was used for all modes. The widths were allowed to vary but remain close to the mean value whatever the nature of the soot. The position of the bands were thoroughly assigned using literature data on hydrocarbonated materials or previous astronomical laboratory analogues (Pendleton & Allamandola 2002; Dartois et al. 2004; Santamaría et al. 2006). Our study focuses on the CH stretch region around 3000 cm^{-1} (3.3 μm) where spectral congestion can be a problem, and the C=C stretch region in which the band is rather isolated from other modes as can be seen in Fig. 2. The characteristics of these bands are reported in Table 1. As a preliminary remark, no strong features due to the presence of oxygen in the material were found (see for instance Fig. 2 around 1720 cm^{-1}). The soots, although produced by burning a hydrocarbon in oxygen, was mainly composed of carbon and hydrogen. Under the rich flame conditions the oxygen is almost completely converted to water and carbon dioxide. In similar experiments, dedicated to soot formation, the elemental analysis showed that the oxygen contamination of the soot was, typically, no more than about 1% (Santamaría et al. 2007).

In all samples bands were found at 3040, 2960, 2925 cm^{-1} and are assigned to aromatic CH, asymmetric aliphatic CH_3 and asymmetric aliphatic CH_2 stretches, respectively (Table 1). Below 2900 cm^{-1} the other identified modes correspond to symmetric stretching modes that are often overlapping. A strong diversity in the intensity ratios between the aromatic and the aliphatic CH stretching bands is observed, as shown in Fig. 2.

Table 1. Infrared band spectral characteristics and assignments as extracted from the soot material samples. The band centres and widths are the mean values found for all the Gaussian fits (see text). The uncertainties are given in parentheses and include the dispersion of the band characteristics. The modes reported here are all stretching (str.) modes.

Assignment	Wavelength (μm)	Wavenumbers (cm^{-1})	Bandwidth (cm^{-1})
Alkyne CH str.	3.040 (0.01)	3289 (10)	39 (10)
Olefinic asym. CH_2 str.	3.24 (0.005)	3089 (4)	25 (5)
Aromatic CH str.	3.29 (0.005)	3039 (4)	49 (10)
Olefinic CH and CH_2 sym. str.	3.35 (0.01)	2981 (10)	25 (7)
Aliphatic asym. CH_3 str.	3.38 (0.006)	2956 (5)	23 (7)
Aliphatic asym. CH_2 str.	3.42 (0.006)	2923 (5)	25 (10)
Aliphatic CH str.			
or aliphatic asym. CH_2 str. Fermi resonance	3.45 (0.012)	2894 (10)	25 (10)
Aliphatic sym. CH_3 str.	3.48 (0.006)	2869 (5)	16 (3)
Aliphatic sym. CH_2 str.	3.51 (0.006)	2850 (5)	13 (3)
	3.53 (0.006)	2834 (10)	29 (15)
sp ² -C=C str.	6.25 (0.1)	1600 (25)	45 (20)

These variations reflect the fact that the flame and sampling conditions can be tuned to produce a wide variety of materials. This is shown by their degree of hydrogenation, which ranges from strongly aromatic CH (sample 1) to strongly aliphatic CH (sample 3). The CH out-of-plane bending mode region below 1000 cm^{-1} does not reveal any strong variations in Fig. 2. However, it was possible to obtain, over the whole range of samples, clear changes in the intensity ratios between the bands at 870 cm^{-1} and 750 cm^{-1} which correspond to solo and quater out-of-plane bending modes, respectively.

The position of the C=C stretch was found to be close to 1600 cm^{-1} and to vary in position over the range 1615–1575 cm^{-1} , i.e. 6.2–6.3 μm , (Table 1). In the 1580–1000 cm^{-1} region (6.3–10 μm) spectral congestion and variations in the band shapes do not allow us to make thorough assignments. The CH bending modes, as well as the CC stretching and bending motions, contribute here but the exact shape depends on the nature of the material. From the information provided by the CH stretching bands, it can be seen in Fig. 2 that the bands are strongly modified from sample 1 to sample 3, i.e. from an aromatic dominated to a strongly aliphatic material.

2.3. Soot structural analysis

The soot is mainly composed of carbon and hydrogen and consists of agglomerated primary particles with diameters of the order of 10–30 nm comprising crystalline and amorphous domains. In general the graphite-like crystalline domains range from single aromatic units to, typically, 3–4 turbostratically stacked graphene layers that could be regarded as highly disordered graphitic lattices (Homann 1998). The global arrangement of these subunits, in onion-like structure for example, depends strongly on the soot itself. No dependence of the band profiles on the sample thickness was observed over more than two orders of magnitude in intensity, the measured infrared transmission spectra can be regarded as the sum of the individual absorption spectra of the primary soot grains under scrutiny, for which the grain size does not affect the infrared spectral features. For such soot grains, the continuum strength and shape should originate from the extent of the carbon network and the inclusion of aromatic units of various sizes in the carbon network. In this sense, the absence of a continuum in some soots dominated by aromatic sub-units would indicate that these are stacked together rather than linked by aliphatic bridges.

Focusing on the CH and C=C stretching modes, as they appear in the FTIR measurements, it is possible to shed some

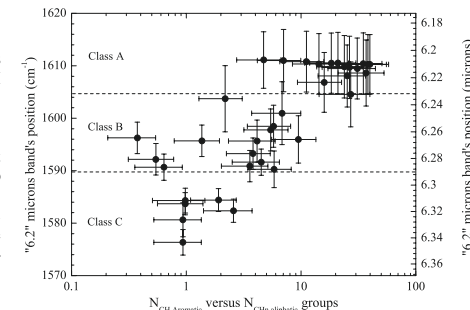


Fig. 3. Evolution of the “6.2 μm ” band position as a function of the aromatic CH bond to aliphatic CH_n group ratio ($N_{\text{CH aromatic}}/N_{\text{CH aliphatic}}$); see text for details) calculated by integration of the optical depth. The horizontal axis is a log scale because the derived values cover two orders of magnitude. The “6.2 μm ” band position shows a clear correlation with the level of substitution and/or presence of the aromatic sub-units. The wavelength ranges of each Aromatic Infrared Band class are as given by Peeters et al. (2002) are plotted.

light on the intimate structure of the soot. The absorption selections for the CH stretches are known from the literature (Dartois et al. 2004) and these invaluable data enable us to quantify the aromatic H versus aliphatic H content, i.e. those contained in the CH_2 and CH_3 groups. From this, the ratio of the aromatic CH bonds, referred to as $N_{\text{CH aromatic}}$, and the number of aliphatic groups, labeled as $N_{\text{CH aliphatic}}$, can be evaluated. $N_{\text{CH aromatic}}/N_{\text{CH aliphatic}}$ is found to vary from 0.3 up to about 40 (Fig. 3) and therefore covers over two orders of magnitude. This provides fundamental insight into the degree of substitution of the aromatic units (in the form of polycyclic aromatic hydrocarbons – PAHs) embedded in the soot (Jones 1990).

A plot of the 6.2 μm band position as a function of $N_{\text{CH aromatic}}/N_{\text{CH aliphatic}}$ is given in Fig. 3 (note the large amplitude on the horizontal scale). The aromatic versus aliphatic content of the material exhibits a clear correlation with the position of the C=C aromatic stretching mode. When the soot is dominated by aromatics, as in sample 1, the band lies at 6.2 μm , and when it is mainly aliphatic, as in sample 3, the band lies at 6.3 μm . The evolution between these extreme positions thus

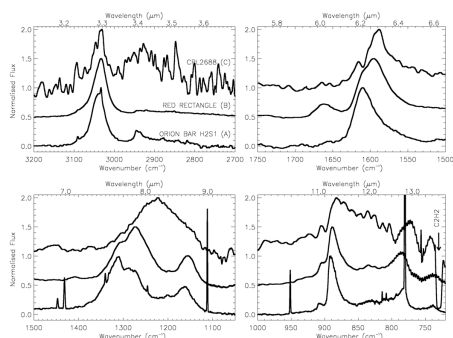


Fig. 4. A selection of three astronomical spectra illustrating the spectroscopic differences encountered in the three spectral classes A–C of the Aromatic Infrared Bands. The spectra have been continuum-subtracted to enhance the spectral profiles, as per Peeters et al. (2002). The same normalisation procedure was applied as in Fig. 2.

appears as a tracer of the carbon skeleton structure. Therefore the position of the C=C aromatic stretching mode reflects an evolution of the environment of the aromatic units embedded in an aliphatic network. Logically, a larger proportion of aliphatics over aromatics should imply the presence of smaller aromatic units and the sensitivity of the C=C bond position to the degree of substitution is expected to be larger when the aromatic units are smaller (Petrie et al. 2003).

From Fig. 3 we can see that the band is found at 6.2 μm when $N_{\text{CH aromatic}}/N_{\text{CH aliphatic}}$ ratio is greater than or equal to 10. The “6.2 μm ” position then reflects a material mainly composed of aromatic units, or clusters of them, linked by very few aliphatic bridges. Although the aromatic units dominate the carbon skeleton in sample 1, we are still far from building up the long range order toward a fully graphitic structure as shown by, for example, the strong band-to-continuum contrast in the recorded spectra. Some evidence for a distribution dominated by small PAHs (up to 32 carbon atoms) comes from Laser Desorption experiments on similar soot samples (Jäger et al. 2006; Apicella et al. 2007). Further studies will help to determine the effective distribution of the PAH-like structures in laboratory soot.

The progressive shift of the band towards 6.3 μm , observed for lower CH ratios, reveals the increasing role of the aliphatic network in defining the carbon skeleton, while the relatively strong intensity of this band shows that the aromatic units remain an intimate component of the soot.

3. Astronomical spectra of interstellar hydrocarbons

3.1. Observations

The continuum-subtracted Short Wavelength Spectra (SWS), from the Infrared Space Observatory (ISO; de Graauw & et al. 1996) database¹, of the Orion Bar H2S1, Red rectangle (HD 441791) and Egg Nebula (CRL2688) are displayed in Fig. 4. The SWS spectra were retrieved using the pipeline processing version OLP10.1 level. Table 2 summarizes the log of

¹ <http://www.iso.vilspa.esa.es/>

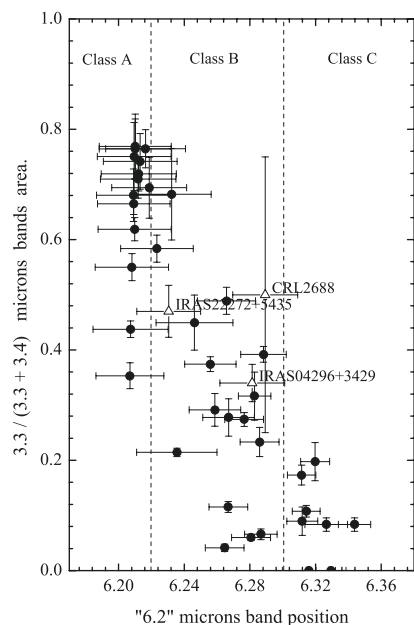


Fig. 5. Dependence of the CH stretching mode region profile as a function of the “6.2 μm ” band position, together with the available astronomical data. The wavelength ranges for each Aromatic Infrared Band class as given by Peeters et al. (2002) are plotted. The filled circles are the laboratory soot data and the open triangle are the astronomical data, the source names are also given.

the observations. A selection based on the Highly Processed Data Products (HPDP) (Sloan et al. 2003) was made and individual orders stitched by applying slight gain corrections (typically less than 10%) using wavelength overlaps. The first three sources in Table 2 illustrate the template line profiles for the three dominant classes of the observed astrophysical AIB spectra (Peeters et al. 2002; van Diedenhoven et al. 2004), the classes A–C.

The ISO spectra of class C sources with available spectroscopic data of sufficient signal-to-noise ratio, IRAS13416–6243, IRAS22272 + 5435, were also extracted. The Spitzer spectrum of the IRAS04293 + 3429 class C source is added to the sample. In addition, we complemented the 3–7 μm infrared space observations (ISO-Spitzer) with more sensitive *L* band (~3–4 μm) ground based spectra of IRAS04296 + 3429, IRAS22272 + 5435 and CRL2688 (Geballe et al. 1992), and IRAS05341 + 0852 (Joblin et al. 1996). With this set of additional data, we are able to explore the aromatic and aliphatic stretching bands fluxes (in the 3.3–3.5 μm range) and the position of the C=C stretching mode (in the 6.2–6.3 μm range). The flux ratios, emitted in the aromatic (3.3 μm) band and normalised to the sum of aromatic plus aliphatic (3.4 μm) stretching band emissions, are used in Fig. 5. The derived ratio is correlated with the extracted C=C line position.

Table 2. Observations.

ISO Source	$\alpha(2000)$	$\delta(2000)$	AOT	Date	Int time (s)	Class
Orion Bar H2S1	05 ^h 35 ^m 20.32 ^s	−05 ^d 25 ^m 19.8 ^s	SWS01/04	1997–10–11	6538	A
HD 441791	06 ^h 19 ^m 58.22 ^s	−10 ^d 38 ^m 15.0 ^s	SWS01/04	1997–10–18	6538	B
CRL2688	21 ^h 02 ^m 18.79 ^s	+36 ^d 41 ^m 37.4 ^s	SWS01/03	1996–11–02	3454	C
CRL2688	21 ^h 02 ^m 18.70 ^s	+36 ^d 41 ^m 36.6 ^s	SWS06	1996–10–20	7962	C
IRAS 13416-6243	13 ^h 45 ^m 07.65 ^s	−62 ^d 58 ^m 19.0 ^s	SWS01/03	1997–08–05	3454	C
IRAS 22272+5435	22 ^h 29 ^m 10.32 ^s	+54 ^d 51 ^m 07.0 ^s	SWS01/02	1996–08–06	1912	C
IRAS 22272+5435	22 ^h 29 ^m 10.27 ^s	+54 ^d 51 ^m 06.4 ^s	SWS01/03	1996–11–17	3454	C
Spitzer						
IRAS 04293+3429	04 ^h 33 ^m 05.7 ^s	+34 ^d 30 ^m 06 ^s	IRS	2005–02–10	25.17	C

3.2. Astronomical spectra

Astronomical sources showing high class A spectra are by far the most dominant by number in the observed AIB spectra. They originate from almost all of the possible photon rich galactic environments (diffuse ISM, Photon Dominated Regions, HII regions, Reflection Nebulae ... etc.). The class C sources are much less represented but correspond to better defined galactic environments, as they are almost always associated with mass-losing stars such as encountered in the post-AGB and Proto-Planetary Nebulae phases. In the CH stretching mode region they display both aromatic and aliphatic emission bands at 3.3 and 3.4 μm , respectively. Class B sources are intermediate cases, not associated with a specific kind of object. In class A and B the spectral energy distribution is generally different from class C sources. In particular, the former sources principally emit the AIBs via stochastic heating followed by infrared fluorescence, whereas for the class C sources grain thermal equilibrium emission is sufficient to explain the observed emission intensities.

The spectra shown in Fig. 4 were obtained by subtracting a continuum in a way similar to that used by e.g. Peeters et al. (2002), using a spline fitting to the sides of the bands, with the spectra taken in $\text{W m}^{-2} \mu\text{m}^{-1}$. Each resulting band emission in the various ranges displayed in Fig. 4 was normalised to its maximum to allow a comparison of the profiles across the distinct A–C classes, to enable us to focus on the spectroscopic profiles. As a consequence a relative comparison of the fluxes emitted in the bands cannot be performed. The corresponding internal energy of class A and B emission lines being much higher than the equilibrium thermal emission of class C, which will for example give strong variations in the 3.3/11.3 μm absolute fluxes.

4. Discussion

4.1. Comparison of laboratory and astronomical data

A comparison of the laboratory soot absorption spectra (Fig. 2) and the astronomical emission spectra (Fig. 4) clearly reveals some similarities. The evolution from sample 1 to 3 resembles that from class A to C. The main disagreement is between the 7.7 μm bands in the class A spectra and the sample 1 spectrum, which brings to mind the main spectroscopic disagreement between the PAH hypothesis and the AIB class A spectra. However, the most striking similarity is the observation of an evolution in the “6.2 μm ” band position from 6.2 μm (sample 1, class A) to 6.3 μm (sample 3, class C). Our interpretation of this similarity is that the position of this band in astronomical spectra traces the nature of the carrier as is observed in the laboratory spectra. This evolution ranges from an aliphatic dominated

material (class C) toward the more matured “astro-PAHs” which are the carrier of the class A AIBs. Note that the exact structures and size distributions of the “astro-PAHs” still remains unclear. It should be noted that the comparison between the spectral characteristics of the soot grains, measured in absorption, and those obtained from the observed emission spectra can be done directly. Effectively several experimental results in absorption and emission have shown that the band shapes and positions for hydrogenated amorphous carbon are not affected by temperature up to almost 800 K (Scott et al. 1997b; Goto et al. 2003), in other words anharmonicity effects do not affect the spectral band characteristics for such grains. In order to build an observable parameter, the ratio between the integrated aromatic CH band at 3.3 μm and the whole CH stretch region (3.3 + 3.4 μm bands) as a function of the 6.2 μm band position is plotted in Fig. 5. The different AIB class wavelength ranges are reported as given in the work by Peeters et al. (2002).

The astronomical data from the selected sources were included in Fig. 5. Actually only three sources have been observed in both wavelength bands, with sufficient spectral coverage and signal-to-noise ratio, that are suitable for our purposes. Two of them are clearly consistent with the observed trend. CRL2688 unfortunately has a large uncertainty in the band ratio. The reason for this is that the observations were made with different instruments, at different spatial resolutions. Therefore the sampling of the source was not homogeneous in the two wavelength bands. However, the laboratory results, built on more than 50 samples, allow an interpretation of the spectral position of the “6.2 μm ” emission band and its use as a tracer of the structure of the emitter. Effectively it outlines the relation between the position of the C=C stretch and the structure of the material as clearly revealed by the CH bonds. It is noteworthy that, to our knowledge, all reported sources with a 6.3 μm band possess aliphatic features.

4.2. Astrophysical implications

Quiescent mass loss from low-mass evolved stars is the primary source of dust in the Milky Way and carbonaceous dust makes up about 40% of the total dust mass budget from these objects (Dwek 1998). By contrast the dust formed around explosive sources, e.g. supernovae, is dominated by oxide/silicate dust formation and the injected mass fraction could be important but is still being debated (Nozawa et al. 2007). Of particular interest for our study are the post-AGB (post-asymptotic giant branch) objects, i.e., sources in transition from the AGB to the planetary nebulae (PN) phase. It is at this stage in the stellar evolution that mass loss has ceased, the dust shell becomes detached from the central star and the stellar and dust emission can be clearly

separated (e.g. Kwok 1993). Generally, the dust becomes optically thin but the stellar radiation is not yet the hard UV field of a PN. Even though the dust shell is detached it appears that hydrocarbon dust formation may still be an ongoing process (Goto et al. 2007).

Carbon-rich protoplanetary nebulae (PPNe), such as those studied by Goto et al. (2002, 2003, 2007), seem to exhibit all AIB spectral classes. However, conversely, these types of source appear to be the only ones to show the class B and C AIB spectra. They are of great interest because the carbonaceous dust responsible for the AIB emission is observed immediately following its formation and it is therefore unprocessed. As PPNe evolve toward the PN phase there is an increase in the intensity and hardness of the UV field accompanied by a temporal evolution of the AIB spectra from aliphatic-dominated to mixed aliphatic/aromatic (e.g. Goto et al. 2002, 2003, 2007). In this scenario the class C AIB spectra, formed in gentle environments free of harsh UV radiation, would appear to be the precursors of the class B and, eventually, the class A spectra (as mentioned by Sloan et al. 2007). The UV radiation field therefore appears to play a crucial role here. However, thanks to observations by Goto et al. (2003), within a given object there is also a spatial evolution of the AIB carriers from aliphatic-rich to aromatic-rich, i.e., the 3.3/3.4 μm fluxes are seen to increase with distance from the central star. How does this spatially varying structural modification occur, is it simply the effect of the interstellar (UV) radiation field dominating over the stellar radiation field a large distance from the star? This could then simply be an analogue of the temporal (source to source) evolution noted above. Does the loss of aliphatic hydrogens then imply a profound structural re-organisation in the fundamental carbon network?

For a long time it has been known that H-rich hydrogenated amorphous carbon films darken upon exposure to UV radiation and that this process of “photodarkening” is accompanied by a decrease in the band gap and the hydrogen content of the material (Watanabe et al. 1982; Dischler et al. 1983; Iida et al. 1985). A similar effect, due to the thermal processing of amorphous hydrocarbons, was interpreted as due to an increase in the aromatic content of the material (Smith 1984; Goto et al. 2000). Thus, laboratory studies show that the photo- and thermal processing of H-rich amorphous hydrocarbons quite naturally lead to the formation and evolution of aromatic or PAH-like structures within the material (e.g. Jones 1990; Scott et al. 1997a; Dartois et al. 2004). Interestingly the 3.4 microns band is also observed in absorption and therefore can be compared to that observed in the class C emission spectra. The bands trace different CH_3 to CH_2 group ratios, which are higher for the hydrogen-rich amorphous carbon seen in absorption and point to a different – i.e. earlier – evolutionary stage in the photo- and thermal processing.

We note that in our sample 1 spectrum, which most closely resembles the class A band profiles, the band shapes are clearly different in the 7.7 and 11.3 μm and longer wavelength regions. Supposing that both the interstellar spectra and the sample 1 spectrum present aromatic-rich end-evolution components, there seems to be some fundamental difference. As noted earlier the band carriers in the class C sources are probably rather large and in thermal equilibrium with the radiation field. However, a rather likely evolution for the interstellar carbonaceous matter (via UV photo-processing, e.g. Goto et al. 2007) is that the size distribution of the emitters evolves in the transition into and in the general ISM, and is subsequently dominated by smaller particles. We thus propose that the differences between sample 1 and class A spectra might principally be due to a size effect and that, in our experiment, the particle sizes remain too large

compared to the interstellar carriers of the bands. It thus seems that our experiments are probably not yet able to isolate and analyse carriers with sizes typical of the IS aromatic-rich band emitters. Galliano et al. (2008) show that within the Galaxy and also in distant galaxies, the ratio of the 6.2 μm /7.7 μm bands (normalised to the 11.3 μm band) in the classical A-type emission band spectrum is essentially constant. This indicates that, in the bright Photon Dominated Regions (PDRs) observed, the carrier of the bands has reached a stable and practically invariant structural composition which is rather aromatic-rich. Our study adds weight to the idea that the main component of the carbonaceous matter in the ISM is rather in the form of aliphatic dominated assemblies composing larger grains, which unfortunately are more difficult to observe.

Our proposed scenario is that these larger grains provide the source for the smaller aromatic-rich species through fragmentation and photo-processing in the ISM (e.g. Jones 2005). These large grains can be observed in emission in the mid-IR because of the rather high equilibrium temperature near the central star (Goto et al. 2007). With increasing distance from the star, the dust temperature decreases and the emission involves a more and more size-dependent mechanism such as stochastic heating by single UV photon absorption. At some stage, only the smaller component can be observed in emission, as is the case for the aromatic-rich (class A) species. Our scenario therefore implies that not all the large grains need to be converted into the “astro-PAHs” because these (parent) large grains simply become unobservable through emission in the mid-IR because they are too cold, unlike the smaller (daughter) “astro-PAHs”. These larger grains would therefore be ejected into the ISM but escape detection in emission. This scenario provides a step toward the missing link between the hydrogenated amorphous carbon component observed in absorption (Dartois & Muñoz-Caro 2007; Dartois et al. 2007) and the more “matured astro-PAHs” observed in emission through the class A (and B) AIBs. It should be emphasized that in IRAS 22272+5435, the carbonaceous dust observed at the position near the central star is largely dominated by the aliphatic component (Goto et al. 2003).

An interesting observable quantity, that would be required to further link the evolution mentioned above and to enable us to quantify what is observed in the astronomical spectra in the CH stretching mode region, would be to perform the same analysis by obtaining the 6.2 μm spectral position as a function of the radial distance in class C sources. Unfortunately this is not yet possible to do. Such studies were recently undertaken in PDRs by Rapacioli et al. (2005); Berné et al. (2007) and showed that a spatial evolution of the AIB spectra could be observed. The carriers labeled as Very Small Grains appeared to emit infrared spectra that clearly resemble sample 2 and 3 spectra (class B and C) and the 6.2 μm band is shifted toward 6.3 μm .

An additional implication, from our self-consistent analysis of laboratory and astrophysical spectra, is that our finding is a better alternative than the need for heteroatoms in heterocycles, such as nitrogen in PANHs as advocated by Hudgins et al. (2005). In the latter work, the evolution from 6.3 to 6.2 μm was proposed to trace the integration of an increasing number of nitrogen atoms in the aromatic carbon skeleton. Two major spectroscopic issues must be addressed as far as the PANHs hypothesis is considered: (i) according to Mattioda et al. (2005); Bernstein et al. (2005), PANHs display another band at about 1400 cm^{-1} (7.14 μm) that is absent in the astronomical data, and (ii) according to the quantum chemical calculations Hudgins et al. (2005), nitrogen atoms must be exclusively toward the centre of the PANHs in order to reproduce the “6.2 μm ” band position.

Such peculiarly strong chemical selectivity is not supported by any mass losing star condensation scenario. In contrast we have shown in this article that a relation exists between the 6.2 μm spectral position and the relative stretching mode ratio intensities $\text{CH}_{\text{aromatic}}/\Sigma\text{CH}$. The production of an aromatic-rich soot that clearly match the class A AIB 6.2 μm band position provides an evolutionary link between the different carbonaceous materials that are observed through the different AIB classes and in PPNe in particular (e.g. Goto et al. 2002, 2003, 2007).

5. Conclusion

An interdisciplinary effort has been made in order to develop dedicated laboratory experiments aimed at producing, characterising and comparing laboratory carbonaceous soots with astronomical spectra. We have performed a consistent analysis of the infrared absorption spectra of more than 50 samples of soot produced under a wide variety of burning conditions, the chemical reactor being a low pressure, flat, rich and premixed flame. From this study, a clear spectroscopic link between the CH stretching mode ratio, the 3.3 versus the 3.4 μm bands, and the position of the C=C aromatic stretching mode, the 6.2 μm band, has been inferred. It underlines the utility of the position of the 6.2 μm emission band to trace the aromatic versus aliphatic content of the carrier. In the light of the classification of the AIBs, the class C appears to be mainly dominated by aliphatic branches linking small aromatic units embedded within the network and the spectral match to a few soot samples is good. Class A spectra carriers are most likely composed of more matured, and perhaps end-evolution, “astro-PAHs” that still await the right laboratory analogues that will provide a good spectral match particularly in both the 7.7 and 11.3 μm regions. In order to clarify the proposed evolutionary scenario between class C carriers and that of class A and B, additional spatially resolved observations of the AIBs in the 6.2 μm band are critically required.

Acknowledgements. The authors would like to thank Dr. Pascale Desgroux and Pr. Katharina Khose-Hoingsang for helpful discussions on the combustion processes in general and the low pressure flames in particular. This work has been supported by the french national program “Physique et Chimie du Milieu Interstellaire” and the French “Agence Nationale de la Recherche” (contract ANR-05-BLAN-0148-02).

References

- Allamandola, L. J., Tielens, G. G. M., & Barker, J. R. 1989, *ApJS*, 71, 733
- Apicella, B., Carpentieri, A., Alfé, M., et al. 2007, *Proceeding of the Combustion Institute*, 31, 547
- Berné, O., Joblin, C., Deville, Y., et al. 2007, *A&A*, 469, 575
- Bernstein, M. P., Mattioda, A. L., Sandford, S. A., & Hudgins, D. M. 2005, *ApJ*, 626, 909
- Bockhorn, H. 1994, *Soot Formation in Combustion: Mechanisms and Models* (Heidelberg: Springer-Verlag)
- Boulanger, F., Abergel, A., Cesarsky, D., et al. 2000, *ISO Beyond Point Sources: Studies of Extended Infrared Emission*, 455, 91
- Buchta, C., D’Alessio, A., D’Anna, A., et al. 1995, *Planet. Space Sci.*, 43, 1227
- Dartois, E., & Muñoz-Caro, G. M. 2007, *A&A*, 476, 1235
- Dartois, E., Muñoz Caro, G. M., Deboffe, D., & d’Hendecourt, L. 2004, *A&A*, 423, L33

- Dartois, E., Geballe, T. R., Pino, T., et al. 2007, *A&A*, 463, 635
- de Graauw, T., Haser, L. N., Beintema, D. A., et al. 1996, *A&A*, 315, L49
- Désert, F.-X., Boulanger, F., & Puget, J. L. 1990, *A&A*, 237, 215
- Dischler, B., Bubbenzer, A., & Koidl, P. 1983, *Appl. Phys. Lett.*, 42, 636
- Draine, B. T., & Li, A. 2007, *ApJ*, 657, 810
- Duley, W. W., & Williams, D. A. 1981, *MNRAS*, 196, 269
- Dwek, E. 1998, *ApJ*, 501, 643
- D’Anna, A., Violi, A., & D’Alessio, A. 2000, *Combustion and Flame*, 121, 418
- Fialkov, A. B., Dennebaum, J., & Homann, K. H. 2001, *Combustion and Flame*, 125, 763
- Flagey, N., Boulanger, F., Verstraete, L., et al. 2006, *A&A*, 453, 969
- Furton, D. G., Laiho, J. W., & Witt, A. N. 1999, *ApJ*, 526, 752
- Galliano, F., Madden, S. C., Tielens, A. G. G. M., Peeters, E., & Jones, A. P. 2008, *ArXiv e-prints*, 801
- Galvez, A., Herflin-Boime, N., Reynaud, C., Clinard, C., & Rouzard, J.-N. 2002, *Carbon*, 40, 2775
- Geballe, T. R., Tielens, A. G. G. M., Kwok, S., & Hrivnak, B. J. 1992, *ApJ*, 387, L89
- Gillett, F. C., Forrest, W. J., & Merrill, K. M. 1973, *ApJ*, 183, 87
- Goto, M., Maihara, T., Terada, H., et al. 2000, *A&AS*, 141, 149
- Goto, M., Kobayashi, N., Terada, H., & Tokunaga, A. T. 2002, *ApJ*, 572, 276
- Goto, M., Gaessler, W., Hayano, Y., et al. 2003, *ApJ*, 589, 419
- Goto, M., Kwok, S., Takami, H., et al. 2007, *ApJ*, 662, 389
- Homann, K.-H. 1998, *Angew. Chem. Int. Ed. Engl.*, 37, 2434
- Hrivnak, B. J., Geballe, T. R., & Kwok, S. 2007, *ApJ*, 662, 1059
- Hudgins, D. M., Bauschlicher, C. W., & Allamandola, L. J. 2005, *ApJ*, 632, 316
- Iida, S., Ohtaki, T., & Seki, T. 1985, in *Optical Effects in Amorphous Semiconductors*
- Jäger, C., Krasnokutski, S., Staicu, A., et al. 2006, *ApJS*, 166, 557
- Joblin, C., Tielens, A. G. G. M., Allamandola, L. J., & Geballe, T. R. 1996, *ApJ*, 458, 610
- Jones, A. P. 1990, *MNRAS*, 247, 305
- Jones, A. P. 2005, in *IAU Symp.*, 235, 124
- Keller, A., Kovacs, R., & Homann, K.-H. 2000, *Phys. Chem. Chem. Phys.*, 2, 1667
- Kwok, S. 1993, *ARA&A*, 31, 63
- Lee, W., & Wdowiak, T. J. 1993, *ApJ*, 410, L127
- Léger, A., & Puget, J. 1984, *A&A*, 137, L5
- Mattioda, A. L., Hudgins, D. M., Bauschlicher, C. W., & Allamandola, L. J. 2005, *Adv. Space Res.*, 36, 156
- Mennella, V., Colangeli, L., & Bussoletti, E. 1995, *A&A*, 295, 165
- Mennella, V., Brucato, J. R., Colangeli, L., & Palumbo, P. 1999, *ApJ*, 524, L71
- Nozawa, T., Kozasa, T., Habe, A., et al. 2007, *ApJ*, 666, 955
- Peeters, E., Hony, S., van Kerckhoven, C., et al. 2002, *A&A*, 390, 1089
- Pendleton, Y. J., & Allamandola, L. J. 2002, *ApJS*, 138, 75
- Petrie, S., Stranger, R., & Duley, W. W. 2003, *ApJ*, 594, 869
- Rapacioli, M., Joblin, C., & Boissel, P. 2005, *A&A*, 429, 193
- Richter, H., & Howard, J. B. 2000, *Progress in Energy and Combustion Science*, 26, 565
- Sandford, S. A., Allamandola, L. J., Tielens, A. G. G. M., et al. 1991, *ApJ*, 371, 607
- Santamaría, A., Mondragón, F., Molina, A., et al. 2006, *Combustion and Flame*, 146, 52
- Santamaría, A., Mondragón, F., Quiñónez, W. E. G., E., & A. F., S. 2007, *Fuel*, 86, 1908
- Schmaiter, M., Mutschke, H., Henning, T., et al. 1996, *ApJ*, 464, L187
- Schmaiter, M., Henning, T., Mutschke, H., et al. 1999, *ApJ*, 519, 687
- Scott, A., & Duley, W. W. 1996, *ApJ*, 472, L123
- Scott, A., Duley, W. W., & Pinho, G. P. 1997a, *ApJ*, 489, L193
- Scott, A. D., Duley, W. W., & Jahani, H. R. 1997b, *ApJ*, 490, L175
- Sloan, G. C., Kraemer, K. E., Price, S. D., & Shipman, R. F. 2003, *ApJS*, 147, 379
- Sloan, G. C., Keller, L. D., Forrest, W. J., et al. 2005, *ApJ*, 632, 956
- Sloan, G. C., Jura, M., Duley, W. W., et al. 2007, *ApJ*, 664, 1144
- Smith, F. W. 1984, *J. Appl. Phys.*, 55, 764
- van Diedenhoven, B., Peeters, E., Van Kerckhoven, C., et al. 2004, *ApJ*, 611, 928
- Watanabe, I., Hasegawa, S., & Kurata, Y. 1982, *Jap. J. Appl. Phys.*, 21, 856
- Weilmünster, P., Keller, A., & Homann, K. H. 1999, *Combustion and Flame*, 116, 62